M-DEM simulation of seismic pounding between adjacent masonry structures

Daniele Malomo [a)] and Matthew J. DeJong [b)]

Abstract: Seismic damage due to pounding between adjacent buildings is often observed after significant earthquake events in old urban centers and globally recognized as a potential trigger for complete collapse. This is relevant for unreinforced masonry (URM) structures, which are particularly vulnerable to horizontal actions and seldom feature appropriate seismic detailing. Quantifying pounding damage between dynamically interacting URM buildings, however, is a challenging task, the details of which are difficult to simulate through analytical modeling alone. Numerical simulation of pounding failures, on the other hand, involves impact, separation and re-contact phenomena that often require advanced 3D micro-modeling strategies, often entailing a high computational expense that is not feasible when modeling the coupled seismic response of multiple buildings. To enable simulation of pounding damage in URM structures with relatively low computational cost, this paper investigates the use of a recently developed Macro-Distinct Element Model (M-DEM) approach. To this end, a M-DEM is herein used to simulate the shake-table biaxial pounding response of two dynamically interacting stone building prototypes, tested within the framework of the Seismic Testing of Adjacent Interacting Masonry Structures (AIMS) project sponsored by the Seismology and Earthquake Engineering Research Infrastructure Alliance for Europe (SERA). Numerical results were obtained before the experimental test and then subsequently evaluated against the experimental results. The M-DEM predictions satisfactorily reproduced the measured base shear and interface opening, although they underestimated the floor displacement demand, especially in the transversal direction. Building on these encouraging outcomes, a post-test refined M-DEM model was also developed, and results are discussed alongside the lessons learned and proposed enhanced strategies to improve the quality of predictions.

1. INTRODUCTION

In high-density old urban centers, buildings were often progressively constructed without being separated by the minimum distance now required for new structures by most modern codes and standards (SA 2007; NTC 2018; ACI 2019). Lack of separation can cause increased earthquake-induced damage due to pounding between adjacent buildings when they oscillate out-of-phase and can result in premature collapse. This is particularly relevant for unreinforced masonry (URM) structures, which are predominant in older districts of most countries, known for their poor performance against lateral loading and identified as the leading cause of seismic fatalities and economic losses globally (So and Spence 2013). As observed during several post-earthquake surveys worldwide (Kasai and Maison 1997; Cole et al. 2010), repeated impacts between URM structures, which seldom feature appropriate seismic detailing, can significantly reduce the in-plane (IP) capacity of piers and therefore reduce global lateral resistance, and can also result in local out-of-plane (OOP) failures (see **Figure 1**). During the 1985 Mexico City Earthquake, Bertero (1986) reported that out of the 330 URM buildings surveyed, 40% exhibited significant pounding damage; in 15% of these cases, pounding was deemed to have triggered a complete structural collapse. However, as noted by Cole et al. (2010), a clear understanding of the risk pounding presents to urban building stock remains elusive.

Figure 1. Pounding damage in URM buildings after the 2011 Christchurch earthquake (Cole et al. 2010)

In the last 30 years, research on seismic pounding has mainly been focused on steel (Sołtysik and Jankowski 2016; Sołtysik et al. 2017), reinforced concrete (RC) structures (Miari et al. 2021; Hosseini et al. 2022) and infrastructure (Won et al. 2015; Sha et al. 2020), as well as on their interaction (Jankowski 2010; Favvata et al. 2013), while only limited studies on URM have been conducted so far. To the authors' knowledge, before the tests conducted by Tomić et al. (2021) in the framework of the Seismic Testing of Adjacent Interacting

Masonry Structures (AIMS) project (sponsored by the Seismology and Earthquake Engineering Research Infrastructure Alliance for Europe, SERA), experimental data pounding URM structures were not available. Previous studies existed instead on different structural systems (Filiatrault et al. 1996; Jankowski 2010), albeit mostly targeting relatively simple linear elastic responses, on which various researchers started to develop fast analytical assessment procedures (Chau et al. 2003; Khatiwada et al. 2013). However, these procedures are not necessarily applicable to URM constructions, given their brittle, highly nonlinear anisotropic behavior and failure mechanisms. Further, dedicated technical guidelines on URM pounding are missing.

Similarly, the literature on the numerical simulation of steel (Sołtysik and Jankowski 2016), RC (Hao 2015; Abdel Raheem et al. 2019) and mixed material structures (Ghandil and Aldaikh 2017; Elwardany et al. 2017) is considerable. In most cases, researchers idealize their case study buildings in an extremely simplified fashion, using either equivalent single-degree-of-freedom (SDOF) (Anagnostopoulos 1988) or fiber-based Finite Element Method (FEM) models, where pounding effects are modeled through contact elements (Khatiwada et al. 2013), mass-dashpot assemblies (Ghandil and Aldaikh 2017) or non-linear impact stiffness interface laws (Davis 1992). In previous URM numerical research, the baseline of modeling complexity is generally higher to account for several factors, including spatial irregularities, influence of diaphragm stiffness and opening layout. Equivalent Frame Models (EFM) (Chen et al. 2008; Penna et al. 2014) appear to be the preferred choice based on the significant number of past contributions, where authors mostly referred to typical European building types in seismic-prone countries (e.g. Italy, Portugal). The reduced computational burden required by EFM models enabled Senaldi et al. (2010) and Pujades et al. (2012) to perform incremental dynamic analyses on multiple adjacent building units, while more recent applications (Formisano and Massimilla 2018; Grillanda et al. 2020; Battaglia et al. 2021) tended to focus on larger assemblies for seismic fragility assessment. In the EFM framework, pounding damage is typically modeled through zero-length interface elements, characterized by linear compression and nonlinear tension softening laws inferred from axial stress-strain and flexural tests on masonry samples (Vanin et al. 2020a). Using this simplified approach, however, interlocking mechanisms and impact damage at wall corners, as well as damage propagation from transversal to longitudinal façades and vice-versa, cannot be accounted for numerically. To account for OOP failures, usually neglected in the EFM methodology and only very recently implemented into their formulation (Vanin et al. 2020b), complex meso (Maniatakis et al. 2018; Sferrazza Papa et al. 2021) and micro-scale (Erdogan et al. 2019; Degli Abbati et al. 2019) FEM approaches have also been applied to the seismic pounding investigation of URM structures, albeit often requiring a significant computational expense, the definition of several experimental and non-physical input parameters, and/or advanced user expertise to interpret and post-process the results obtained. Further, with FEM models, despite having the ability to represent damage initiation and propagation more directly, it is usually challenging to simulate the impact , separation and re-contact phenomena typically involved in pounding failures. On the other hand, the employment of Distinct Element Method (DEM) approaches (Cundall 1971), which are naturally suitable for modeling the dynamic interaction among discrete bodies and have been successfully used for simulating reduced-scale URM assemblies (Pulatsu et al. 2016), are often not feasible due to prohibitive analysis times. In this work, to overcome the abovementioned difficulties and combine the efficiency of simplified approaches with the multifaceted capabilities of DEM methods, the adequacy of a new Macro-Distinct Element Model (M-DEM) developed by the authors to simulate the seismic pounding of complex URM structures is evaluated. To this end, the modeling strategy was adopted and the numerical analysis was performed before the SERA-AIMS tests, whose details are discussed in the next sections. Subsequently, after the test, simulation and laboratory results were compared and are discussed herein. Finally, additional post-test simulations were conducted and evaluated to improve the modeling strategy.

2. M-DEM FOR THE SEISMIC ANALYSIS OF URM STRUCTURES

According to the original M-DEM formulation, each URM member is idealized as an assembly of six deformable FE macro-blocks (see **Figure 2** (a)), characterized by an internal tetrahedral mesh and connected to each other by horizontal, vertical and diagonal nonlinear spring layers, whose number and layout are determined *a priori* as a function of aspect ratio λ_w (calculated as h_w/l_w, i.e. wall height over its length, see **Figure 2** (b)) and masonry texture. Variations to this initial scheme can easily be introduced to model more complex behaviors, e.g. different boundary conditions (see Malomo and DeJong (2021b). The M-DEM has been comprehensively validated against IP, OOP and combined seismic loading tests on both brick and concrete block URM building components and sub-systems (Malomo and DeJong 2021b, a, c). The novelty of the work presented herein thus lies in the extension to the modeling of the stone masonry material at a larger scale and higher complexity (in previous papers, only isolated façades and assemblies without diaphragms were considered), as well as to seismic pounding damage simulation (beyond the scope of past contributions).

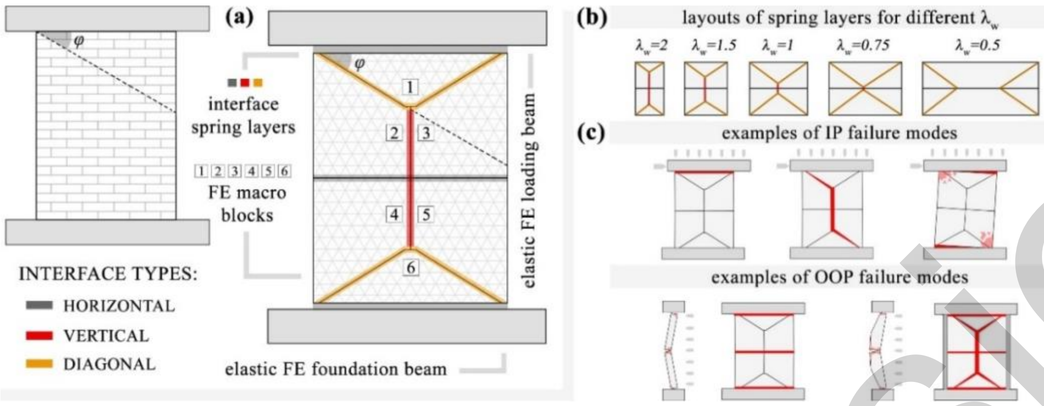

Figure 2: (a) M-DEM idealization, (b) spring layers as a function of the aspect ratio, (c) IP/OOP failures

The average slope (φ) of the lines connecting consecutive head joints along the height/length of a given masonry element (Malomo et al. 2019a) is used to define potential failure planes for the development of discrete cracks between the FE blocks. Such a simplified discretization scheme, exhaustively discussed in Malomo and DeJong (2021c), was devised for reproducing the main failure modes typically observed during experimental IP tests on both URM spandrel (Beyer and Dazio 2012) and wall (Magenes and Calvi 1997) components. Note that is not necessary to assume the effective height of piers, which is one limitation of EFM models. Meanwhile, as qualitatively shown in **Figure 2** (c) and demonstrated in Malomo and DeJong (2021a), it also enables the possibility of simulating the main OOP collapse modes under both one-way (Penner and Elwood 2016) and two-way (Griffith et al. 2007) bending. Shear and tensile failures are accounted for by the interface springs, characterized by a Mohr-Coulomb criterion with tension cut-off (see **Figure 3** (a)) and to which normal (k_n) and tangential (k_s) dummy stiffnesses are assigned. Shear and tensile post-peak softening branches were not considered herein. In shear, as depicted in **Figure 3** (a), the contribution of cohesion is lost right after the maximum shear stress, while that of dry friction remains constant. Tensile strength is set to zero after the attainment of the maximum allowable normal stress. These simplified assumptions typically yield reasonable but conservative results when simulating the seismic response of large-scale masonry constructions (Karbassi and Nollet 2013; Malomo et al. 2020a), albeit not representative of the actual quasi-static (post-peak responses of brittle materials can only be recorded when applying very low velocities) micro-scale behavior of masonry assemblies, as demonstrated experimentally by Van der Pluijm (1993, 1997). Recent advances in DEM now offer more rigorous solutions for contact modeling of masonry structures (Pulatsu et al. 2019, 2020), whose compatibility with the M-DEM approach is currently being explored. While friction angle ϕ, cohesion c and tensile strength f_t of horizontal joints are assumed equal to those inferred through triplet and bond wrench tests respectively, equivalent values (i.e. $\bar{\phi}, \bar{c}, \bar{f_t}$) are calculated for the diagonal joints as a function of φ, using Equations (1), (2), (3). On the other hand, the equivalent shear/tensile strength parameter (i.e. $\bar{\bar{c}} = \bar{\bar{f_t}}$, Equation (4)) proposed by Beyer (2012), evaluated also considering the resistance provided by interlocking units (with thickness t_u, length l_u and width w_u), is specified for the t_j-thick vertical joints.

$$\textbf{(1)}\quad \bar{\phi} = \frac{\phi\cos(\varphi) + \sin(\varphi)}{\cos(\varphi) - \phi\sin(\varphi)} \qquad \textbf{(2)}\quad \bar{c} = \frac{c\cos(\varphi)}{\cos(\varphi) - \phi\sin(\varphi)} \qquad \textbf{(3)}\quad \bar{f_t} = \frac{f_t}{\cos(\varphi)} \qquad \textbf{(4)}\quad \bar{\bar{f_t}} = \frac{c(t_u + t_j) + (l_u\phi)(\phi + c)/1.5}{2\phi(t_u + t_j)}$$

A linearized version of the Feenstra and De Borst (1996) strain-softening compression model (**Figure 3** (b)), initially conceived for simulating concrete, was implemented into 3DEC (Itasca, 2013) and assigned to the FE blocks to account for masonry crushing. Further, the explicit time-integration scheme on which the selected computational platform is founded makes the M-DEM compatible with seismic pounding analysis.

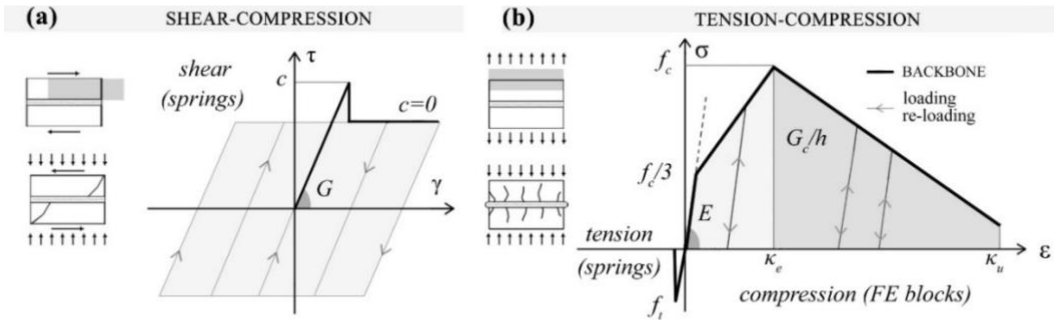

Figure 3: (a) Tension-compression and (b) shear-compression M-DEM constitutive laws

As it can be gathered from **Figure 3**, stiffness degradation is not explicitly included in the M-DEM contact models, nor in the adopted FE crushing failure criterion. However, as discussed in e.g. Malomo et al. (2019b) and Malomo et al. (2020b), this phenomenon is implicitly accounted for numerically through the progressive failure of interface springs in tension and FE zones in compression. This simplified approach is one of the aspects making contact-based models more suitable for simulating separation and re-contact phenomena with respect to e.g. smeared crack FE approaches with complex cyclic stress-strain relationships, requiring only basic plastic interface parameters (D'Altri et al. 2020).

3. BRIEF DESCRIPTION OF THE SERA-AIMS BUILDING SPECIMEN

The building specimen was constructed and tested at the National Laboratory for Civil Engineering (LNEC – Lisbon, Portugal) in November 2021. It consisted of two half-scale adjacent masonry units (hereinafter referred to as unit 1, U1, and unit 2, U2, see **Figure 3** (a, b)) separated by a dry joint interface (no interlocking), with a total mass of 23.7 tons (U1 7.4 tons, U2 16.3 tons), excluding foundations. U2 had two levels, four 0.3 m-thick double-leaf stone masonry walls and plan outer dimensions of 2.5 x 2.5 m^2. The total height was 3.15 m and an additional 1.5 tons was uniformly distributed on each level. U1 was U-shaped in plan, with three walls (same type and thickness as U2). It was constructed with the same materials and plan dimensions. Both units were characterized by flexible timber diaphragms composed of 0.08 m x 0.16 m joists connected to 2 cm thick floor planks. The joists of U1 spanned in the *x*-direction, while the joists of U2 spanned in the *y*-direction.

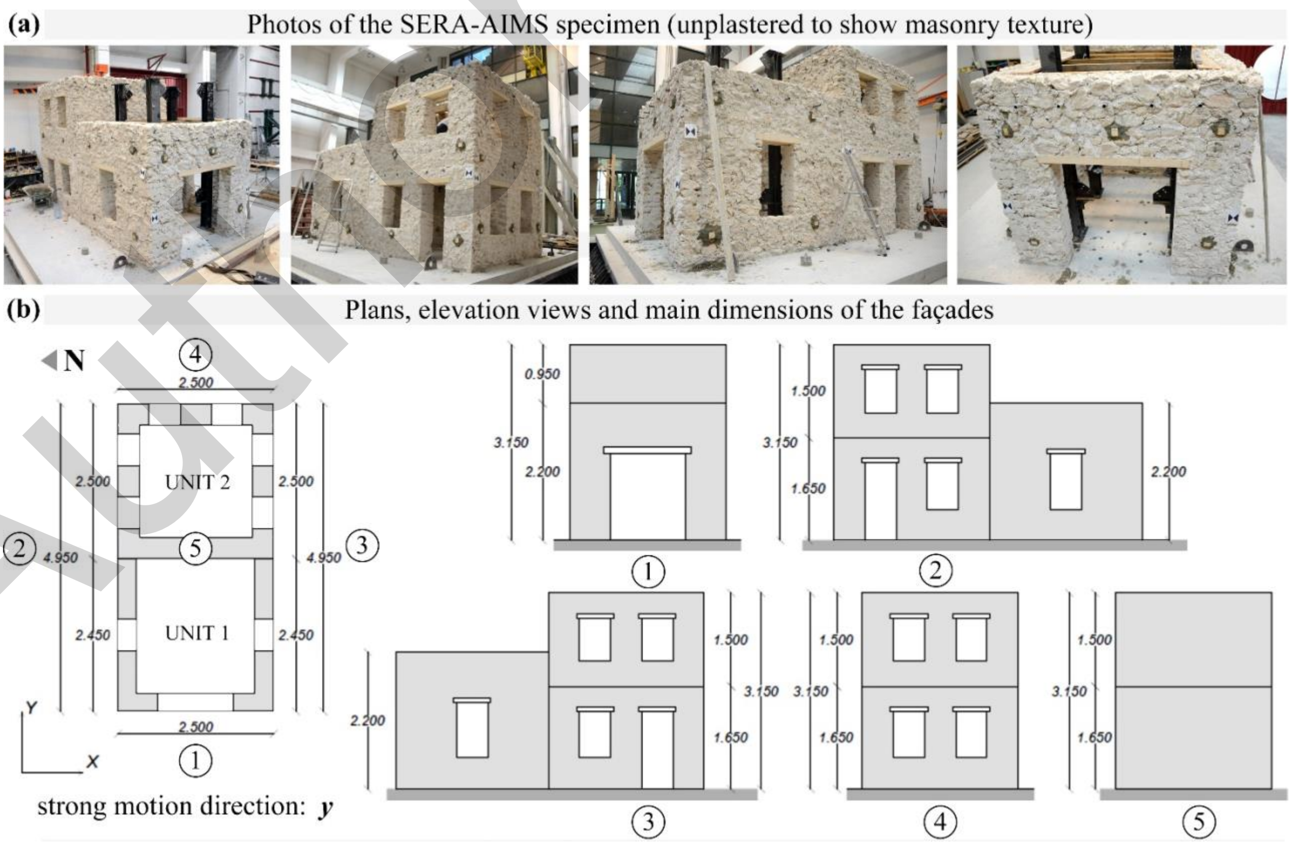

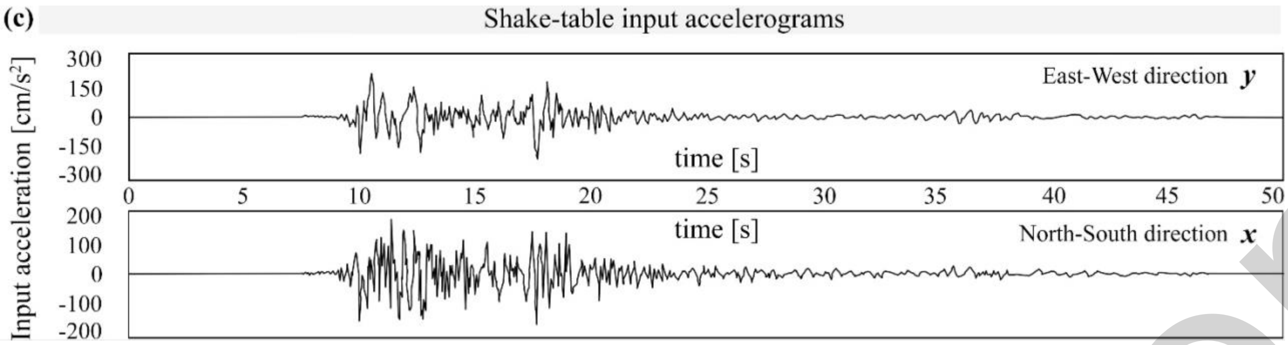

Figure 3: (a) Photos and (b) plans/elevation views of the specimen, (c) shake-table input accelerograms used during the test (adapted from Tomić et al. 2021)

As shown in **Figure 3** (c), two different accelerograms recorded during the 1979 Montenegro earthquake (Luzi et al. 2020) were scaled and applied to the shake table, either individually or simultaneously in orthogonal directions. The loading protocol used in pre-test simulations was slightly different from the loading protocol used in the lab. The considered testing sequences are given alongside numerical results in the next sections, together with assumed (pre-test) and actual (post-test) masonry properties. The building specimen was retrofitted after relevant damage was observed during testing; as this paper only refers to the unretrofitted configuration and test results, this will not be discussed here. Interested readers are referred to Tomić et al. (2021) for further details, where a more comprehensive test description is provided.

4. M-DEM IDEALIZATION OF STRUCTURAL DETAILS AND KEY ASSUMPTIONS

In previous research contributions, the M-DEM was used to simulate clay brick and concrete block URM assemblies, so the modeling of stone masonry required the definition of new idealization schemes and assumptions and resulted in several modeling challenges (labeled I to VI). The main source of these challenges was the heterogeneity of the masonry elements (see **Figure 4**), where two adjacent leaves of irregular stones of similar yet different dimensions were assembled by mortar joints of varying thickness. Indeed, (I) the definition of the average slope φ (essential for discretizing the M-DEM panels) in this case is not trivial, and its determination would ideally involve an in-depth statistical study of the actual masonry texture (Zhang et al. 2018) – something that was not possible before the tests and that would have implied a prohibitive effort in the post-test calibration. Other key challenges included: (II) the selection of masonry material properties, (III) the modeling of flexible timber diaphragms, (IV) the modeling of lintels (**Figure 4** (a, b)), (V) the modeling of interlocking corners (**Figure 4** (a, c)), and (VI) the determination of a proper damping scheme.

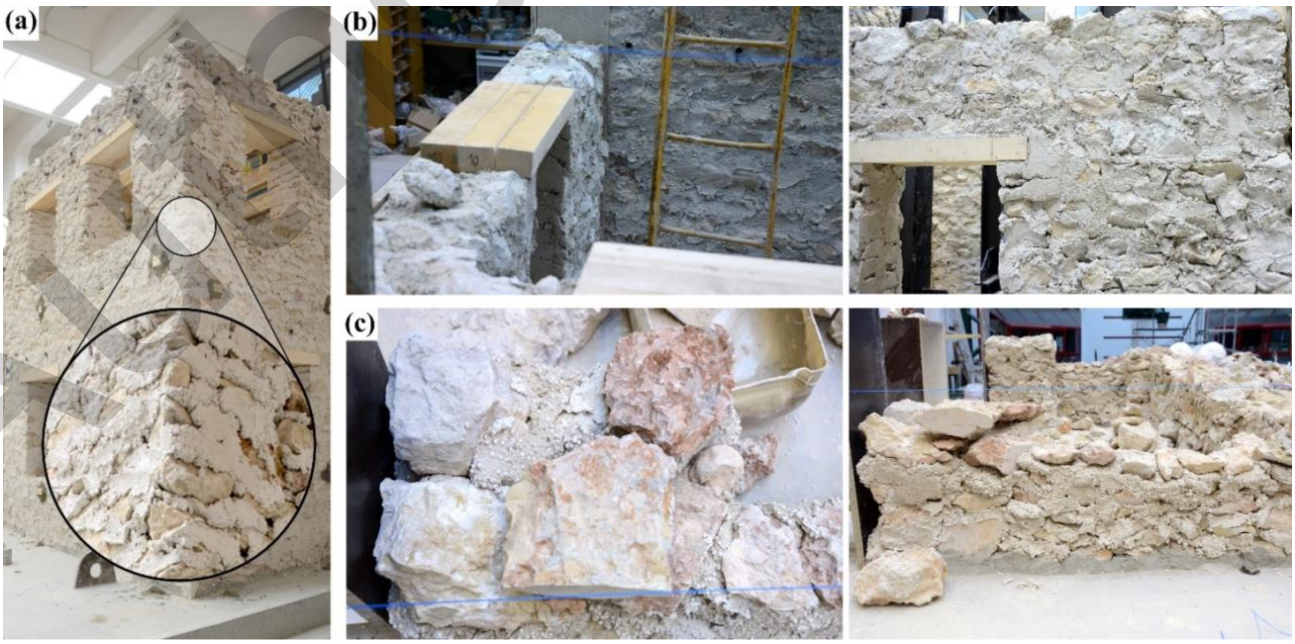

Figure 4 (a) Zoom on N-W corner, (b) lintels and (c) masonry details (adapted from Tomić et al. 2021)

In what follows, the solutions adopted to the issues mentioned and numbered (I-VI) above are discussed:

I) *The average slope* φ was defined by calculating the approximate average crack inclinations suffered by the half-scale building specimen tested by Guerrini et al. (2019). The specimen was subjected to incremental shake-table motion in 2019 at the laboratory of Eucentre (Pavia, Italy), as part of a previous research program led by some of the principal investigators of the SERA-AIMS project. This previous test shared similar characteristics with the masonry units tested in this study, including the masonry type. The estimated φ ($\approx 45°$) was also representative of the inclination of the diagonal shear cracks observed by Senaldi et al. in 2018, who tested walls under quasi-static IP loading – the responses of these walls have been replicated numerically with the M-DEM to substantiate the simplified assumption above, obtaining satisfactory results (see next section). As shown in **Figure 5**, the definition of φ enabled discretization of the building specimen in M-DEM spandrel, pier and deformable node elements as proposed in Malomo and DeJong (2021c).

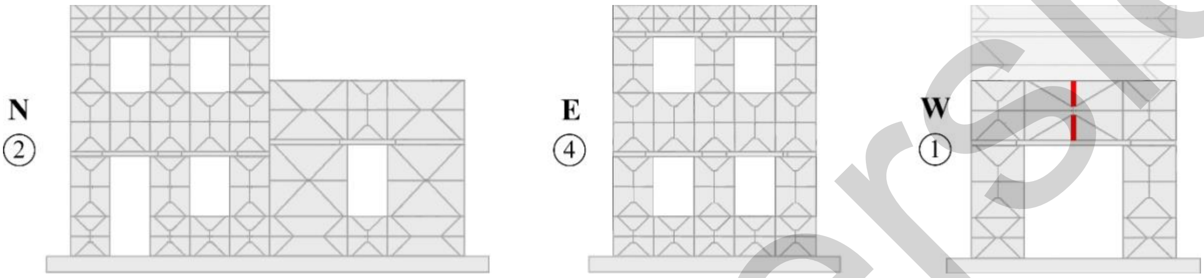

Figure 5 M-DEM discretization of the SERA-AIMS building specimen

Although the original algorithm (see Malomo and DeJong 2021c) used for generating M-DEM discretization schemes determines number and layout of joint interfaces *a priori* as a function of aspect ratio λ_w (see **Figure 2**(b)), the central top spandrel (free top edge) of the West façade of U1 (**Figure 5**) features a further vertical subdivision of bottom and top FE macro-blocks (highlighted in red in **Figure 5**). This simple modification, recently validated in Malomo and DeJong (2021b) against experimental tests on URM, was introduced for capturing potential OOP failures in the pre-test phase (not observed experimentally though), not possible with the original discretization that only considers simply-supported and fixed-fixed OOP conditions. Based on the dimensions and diaphragm orientation of the top West walls of U2, this more refined subdivision was not applied to those elements.

II) *Selecting appropriate stone masonry properties* is vital for obtaining acceptable numerical results, and particularly challenging when using interface-based models employing the Mohr-Coulomb failure criterion, as in the M-DEM. In fact, input parameters considered for brick and block URM assemblies, such as the friction coefficient, cohesion c and tensile strength f_t, are difficult to infer experimentally for irregular stone masonry, and not necessarily representative of its actual behavior due to complex interlocking phenomena (Calderini et al. 2010). It is not uncommon, indeed, to experimentally obtain a large range of friction angles ϕ between 30° and 65°, corresponding to coefficients μ of 0.6 and 2, respectively (Milosevic et al. 2013). Based on previous tests on similar masonry types (Binda et al. 1994; Vasconcelos and Lourenço 2009; Elmenshawi and Shrive 2015), ϕ=35° (μ=0.7) was adopted in this work. Similar values of ϕ (ranging from 31° to 38°, i.e. μ=0.6-0.8), not determined in the SERA-AIMS project, were also successfully used by various researchers simulating the seismic response of analogous stone masonries (e.g. Chácara et al. 2018; Lemos and Campos Costa 2017). For the selection of reasonable cohesion and tensile strength values, reference was made to the results of diagonal compression tests conducted by Senaldi et al. (2018) for the pre-test simulations. These parameters were then modified for the post-test modeling using the data made available by Tomić et al. (2022), assuming $c = \tau_{max}$ and $f_t = \sigma_t$ (as shown in **Table 1**, post-diction values were ≈ 20% larger than the pre-test ones). For the compressive strength f_c and Young's modulus E_m of masonry, values obtained by Senaldi et al. (2018) through uniaxial cyclic compression tests on masonry wallettes were considered for the pre-test model, and these were then decreased by 25%-30% for the post-test simulations, based on the new parameters inferred by Tomić et al. (2022). From the Senaldi et al. (2018) tests, the shear modulus of masonry G_m was also given as part of the blind prediction information package (no updated G_m was provided for the post-test analyses, where G_m was set to 1352 MPa assuming the same pre-test G_m/E_m ratio of 0.548, with the new E_m=2467). In **Table 1**, experimental (identified with the symbol *) and M-DEM masonry properties are summarized. The fracture energy G_c was estimated using a modified expression from CEB/FIP Model Code 90 (Comite Euro-International Du Beton 1990) adapted by Lourenço and Pereira (2018) to lower-strength masonries where $G_c = 2.8 f_c - 0.1 f_c^{\,2}$. In addition to the abovementioned properties, dry-friction nonlinear parameters ($c = f_t = 0$, $\phi = 35°$) were assigned to the interface between U1 and U2 of both pre- and post-test models, to simulate their dynamic interaction. These zero-length springs failed in tension-shear in the very first steps of the dynamic analysis, providing only residual shear frictional resistance, thus replicating in a reasonable way the mechanics of the dry joint (no interlocking) used in the test for separating the two units, also cracked in the early stages of shake-table testing.

Table 1 Measured masonry material properties and equivalent pre/post-test M-DEM parameters

	*E_m	*G_m	k_n	k_s	*f_c	*f_t	*c	ϕ	φ	$\bar{f}_t$	$\bar{c}$	$\bar{\phi}$	$\bar{\bar{c}} = \bar{\bar{f}}_t$	G_c
	[MPa]	[MPa]	[MPa/mm]	[MPa/mm]	[MPa]	[MPa]	[MPa]	[°]	[°]	[MPa]	[MPa]	[°]	[MPa]	[N/mm]
Pre-test	3462	1898	346.2	189.8	1.75	0.17	0.23	35	45	0.24	0.77	79.91	0.41	4.59
Post-test	2467	[1]1352	[2]24.67	135.2	1.28	0.21	0.29	35	45	0.30	0.97	79.91	0.47	3.42

[1] Experimental E_m and G_m values were directly assigned to FE blocks. G_m was set to $0.548E_m$ after the test, assuming the same pre-test G_m/E_m ratio
[2] As explained in Section 7, k_n of the post-test models was decreased by a factor of 10 to account for the presence of voids between masonry stones

III) To model in a simplified fashion the *in-plane stiffness of the flexible timber diaphragms*, the latter have been idealized as an assembly of linear elastic isotropic solid beams (each divided into tetrahedral FE with maximum element length EL=0.25 m), to which basic elastic properties of timber were assigned (i.e. Young's modulus of 12 GPa and a density ρ_m of 450 kg/m^3) connected by crossed diagonal links (see **Figure 6** (a)), each featuring an equivalent axial stiffness K_α. Each pair of crossed diagonal links, discretized in ≈0.1 m-long FE, accounted for the in-plane stiffness K_d of the portion of diaphragm of span B comprised by n_j=2 consecutive joists, calculated analytically considering their different orientation, as proposed by Gattesco and Macorini (2014). Needed parameters were inferred using Equations (5), (6) and (7) below, where k_{ser} is the slip modulus of a nail of diameter ϕ_n as per Eurocode 5 (2005), s_n is nail spacing, n_b is the number of planks and α is the link-to-beam angle

(5) $$k_{ser} = \left(\frac{\rho_m^{\,1.5}\,\phi_n^{\,0.8}}{30}\right)$$ **(6)** $$K_d = \left(\frac{n_j\, n_b\, k_{ser} s_n^{\,2}}{2B^2}\right)$$ **(7)** $$K_\alpha = K_d(\cos\alpha)^2$$

To assess the reliability of the proposed diaphragm modeling approach before performing pre-test simulations, preliminary analyses were performed on floor sub-structures to measure analytical vs numerical elastic vertical deflections under self-weight and overall IP stiffness, obtaining marginal differences for both cases (<10%). In **Table 2**, the values obtained and then adopted for the pre and post-test models are summarized.

Table 2 Measured masonry material properties and equivalent pre/post-test M-DEM parameters

	H [m]	n_j [-]	n_b [-]	α [°]	ρ_m [kg/m^3]	ϕ_n [m]	s_n [m]	k_{ser} [N/mm]	K_d [kN/m]	K_α [kN/m]
U1 - roof	1.98	2	10	15.5	450	0.003	0.15	766	109	42
U2 - floor	0.32	2	1.5	12.6	450	0.003	0.15	766	123	253
U2 - roof	0.38	2	2	14	450	0.003	0.15	766	111	216

IV) As shown in **Figure 4** (a, b), the SERA-AIMS specimen featured *timber lintels* embedded into the masonry by approximately 0.1-0.15 m. The same material assigned to timber joist was herein used for lintels, modeled as linear elastic isotropic beams. Their introduction, however, required the addition of special "filling elements", highlighted in red color in **Figure 6** (a), to which the same properties of other FE masonry blocks were assigned. **Figure 5** displays their interaction with M-DEM panels.

V) **Figure 4** (a, c) shows that *stones at corners were interlocked* in the building specimen. To reproduce this numerically, the simplified strategy shown in **Figure 6** (b) was adopted. This also enabled us to apply independently on each façade the M-DEM discretization, while allowing a more realistic 3D propagation of cracks around corners. Alternatives to this approach were implemented into the post-test model, as per the recent developments presented in (Malomo and DeJong 2021b).

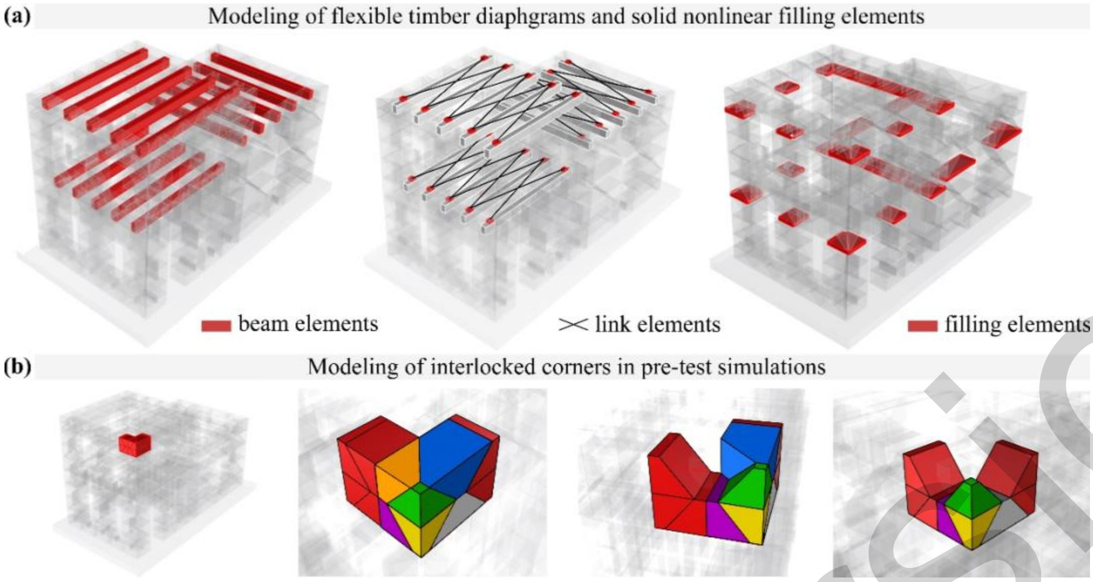

Figure 6 (a) Idealization of flexible diaphragms and filling elements, (b) modeling of interlocking corners

VI) In DEM simulation, researchers have used various *damping schemes* to model the seismic response of URM structures, ranging from zero (Malomo et al. 2021) to stiffness proportional (Malomo and DeJong 2021a), mass proportional (Çaktı et al. 2016) or combined (e.g. Rayleigh, see Kim et al. 2021) damping. Both analytical studies (DeJong 2009) and comparisons with test results seem to suggest that zero damping or only stiffness proportional damping (Malomo and DeJong 2021b) are more appropriate for URM simulation, particularly when rocking and subsequent OOP overturning collapse occurs. However, the analysis time increases dramatically using these two options as the time-step exponentially decreases. Additionally, when material damping is important and the response is less dominated by large displacement rocking behavior, Rayleigh (i.e. combined) damping is widely considered as effective. For these reasons, especially when dealing with large computational models (as noted by Lemos and Campos Costa 2017), mass-proportional damping provides some benefits. To investigate the implications of distinct types of damping on the expected computational expense, a parametric study including various types of damping schemes was conducted before the test with the M-DEM model. A free vibration numerical test (a linearly increasing velocity was applied at the base and then abruptly removed) was first performed (an eigenvalue analysis can only be done when using rigid blocks in 3DEC, not an option using the M-DEM approach as macro-blocks are deformable) to estimate the natural frequency f_n to be associated the applied fraction of critical damping ζ. Natural frequencies of 18 Hz and 22 Hz were obtained for modes I and III respectively, using the Fast Fourier Transform. Slightly lower values were estimated along the *x*-direction. Fictitious (large) values of f_n were selected for the stiffness-proportional case, as suggested by DeJong (2009). Based on the analysis time results of **Table 3**, where it can be observed how the analysis time exponentially increases when the stiffness-proportional damping component is present, it was decided to proceed with mass proportional damping with ζ = 4% at 18 Hz. Previous experimental (Elmenshawi et al. 2010; Elmenshawi and Shrive 2015) and numerical (Pelà et al. 2009; Penna et al. 2016) studies on stone masonry structures inferred/assumed similar values, between 2 to 4%. To further increase the time-step t and reduce the analysis time, as some FE mesh elements were small (maximum mesh length was 0.4 m, but several elements were below 0.01 m because of the tetrahedral zoning) with relatively low masses, their density was artificially reduced by an iteratively determined value (ρ_s = 7%) using the partial density scaling devised by Cundall (1982) and currently implemented in 3DEC (after the users specify the ρ_s target value, the scaling process is fully automated) that ensures negligible changes of system inertia.

Table 3 Damping schemes (setting adopted in pre-post models in gray color) and analysis runtime

Damping scheme	ρ_s [%]	f_n [Hz]	ζ [%]	t [-]	*Expected analysis time per second* [h]	*Analysis time of each case vs reference ones* [-]
stiffness-proportional	7	1000	100	3.2e-8	78	x156
stiffness-proportional	7	3000	100	9.5e-8	24	x48
stiffness-proportional	7	10000	100	3.2e-7	7.5	x15

mass-proportional	7	18	4	4.5e-6	0.5	reference value
mass-proportional	7	18	2	4.5e-6	0.5	reference value
Rayleigh	7	20	4	3.1e-8	76	x152
Rayleigh	7	20	2	6.4e-8	38	x76
Rayleigh	7	43	3	9.2e-8	26	x52

5. PRELIMINARY VALIDATION AGAINST IN-PLANE WALL TESTS

To validate the modeling strategy and assumptions I-II discussed in the previous section before the test, the IP cyclic shear-compression responses of a squat (CT01, ratio *h/l* of pier height *h* to length *l* equal to 1.26; *h*=1.45 m, *l*=1.15 m) and slender (CS01, *h/l*=3; *h*=1.80 m, *l*=0.6 m) half-scale stone masonry walls characterized by similar properties of those of the SERA-AIMS project were reproduced numerically. The walls, tested by Senaldi et al. in 2018 at the Eucentre laboratory, were subjected to quasi-static loading protocols under fixed-fixed boundary conditions. A vertical overburden of 0.4 MPa was applied and kept constant using two servo-hydraulic actuators connected to the lab strong walls and top RC beams. As shown in **Figure 7** (a), wall CT01 failed in diagonal shear with cracks inclined at 35-55°, exhibiting crushing at the toe and a marked stiffness and strength degradation, while the behavior of CS01 was dominated by rocking and heel crushing; the crushing explains the relatively large dissipated energy for rocking failure that was recorded experimentally. Given the variety of different failure mechanisms exhibited by the wall specimens and the similar masonry, CT01 and CS01 were taken as a reference and modeled using the M-DEM. The inclination of CT01 cracks guided the calibration of φ, which was set to 45°, corresponding to the best match obtained with experimental results. Different FE mesh sizes characterized by varying maximum element length EL were tested, ranging from EL=0.1 m to EL=0.4 m. Similar to the results in Malomo and DeJong (2021c) modeling clay brick walls, the employment of different EL values only affected shear-governed results, particularly during final cycles when damage was significant. As shown in **Figure 7** (b) though, predictions obtained using upper (EL=0.4 m) and lower (EL=0.1) bound EL are both comparable with experimental hysteretic curves and damage distribution. Model CT01-EL01 (i.e. M-DEM model of CT01 using EL=0.1 m) adequately estimated initial stiffness (ratio between numerical and test values at 15% of maximum base shear, rK, is equal to 0.87) and average peak base shear BS_p (ratio rBS_p=0.93), while overestimating total dissipated energy E_h (ratio rE_h=1.21). Very similar values were inferred using CT01-EL04 (rK=0.88, rBS_p=0.96, rE_h=1.07), which generally provided slightly better approximations. As per the CS01 models, minor differences were observed between CS01-EL04 (rK=1.02, rBS_p=1.11, rE_h=1.33) and CS01-EL01 (rK=1.09, rBS_p=1.16, rE_h=1.19) albeit both satisfactorily captured the overall experimental response measured in the lab, including crushing-induced E_h, which is challenging for most interface-based numerical models (Penna et al. 2014; D'Altri et al. 2019). Given the adequate results obtained, assumptions I and II were confirmed and EL=0.4 was used for all models without any post-test adjustments, as discussed below.

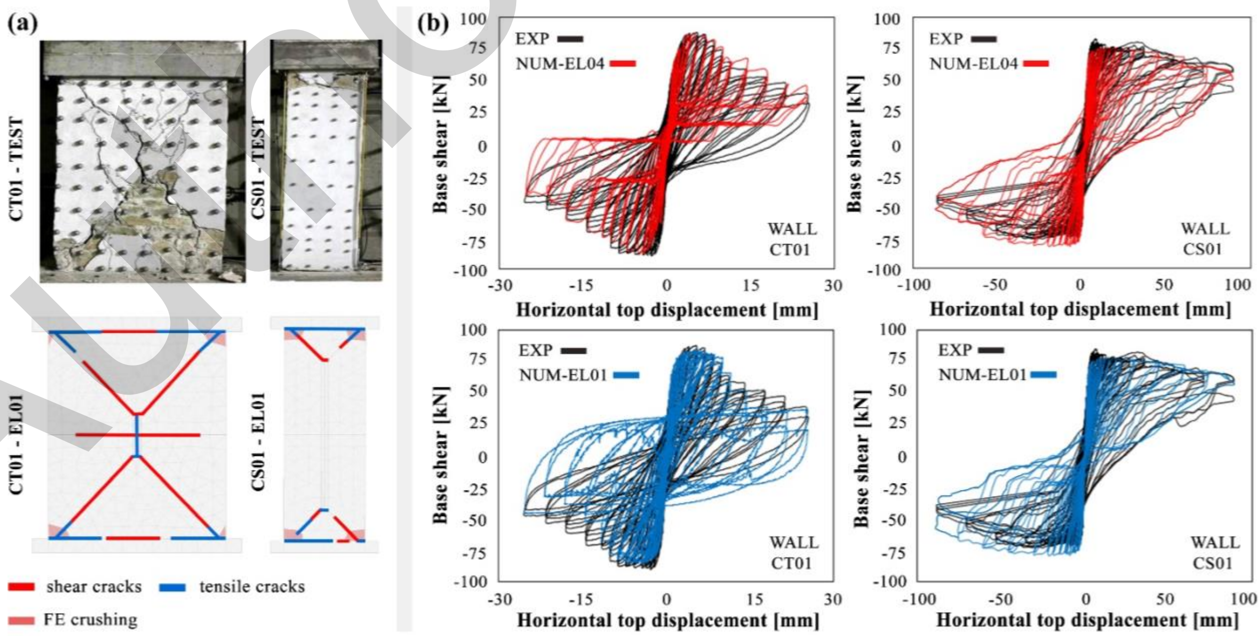

Figure 7 Test (adapted from Senaldi et al. 2018) vs numerical (a) damage and (b) hysteretic response

6. PRE-TEST NUMERICAL PREDICTIONS

In this section, the main numerical results obtained before the test in the framework of the SERA-AIMS blind prediction exercise are presented and discussed. The model, depicted in **Figure 8** (a), was developed according to the strategy described in the preceding sections. EL=0.4 m was adopted for the internal mesh of the FE macro-blocks (**Figure 8**(b)), to which the mechanical properties of the stone masonry were assigned. Lintels and floor joists were modeled as solid linear elastic beams with reference timber elastic material parameters, see **Figure** 8(c) (link elements were hidden for clarity). As shown in **Figure 3** (c), the employed shake-table seismic records had an effective duration of about 40 seconds. In both pre and post-test M-DEM models, *x*- and *y*-direction signals applied were truncated to further reduce analysis time. The portion of the records used starts at 3.66 seconds and ends at 16.67 seconds, for a total duration of approximately 13 seconds. This strategy, which enabled us to reduce computational expense by more than 200%, was implemented following an in-depth signal analysis in SeismoSignal (Antoniou and Pinho 2004), to minimize potential undesired dynamic effects.

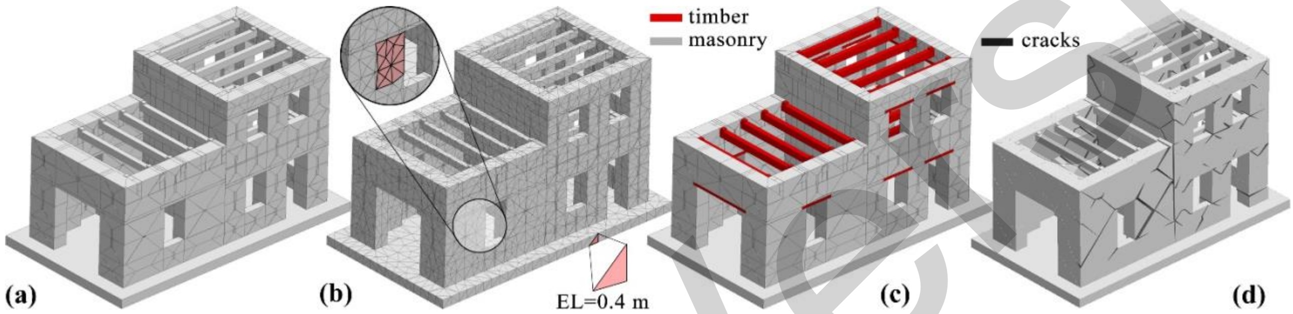

Figure 8 (a) Screenshot of the model, (b) FE mesh, (c) material distribution, (d) final predicted damage

The pre-test loading sequence employed is reported in **Table 4**, and characterized by four main phases where uniaxial X, Y, and biaxial X-Y shakings were alternated. The whole shake-table test sequence was applied subsequentially to the model, enabling us to consider explicitly damage accumulation. It is noted that the peak table acceleration (PTA) for each run and other characteristics of the signal imposed to the building specimen were changed during the test, as discussed in the next section. Similarly, the specimen was retrofitted (floor and roof strengthening of U2) after test 2.1 (actual PTA=0.593g) to avoid premature collapse, an unpredictable scenario that could not be accounted for numerically before the test. The pre-test M-DEM model used for the blind prediction exercise and to which the pre-test loading protocol of **Table 4** was applied was thus unretrofitted. Therefore, pre-test numerical results after run 2.1 (nominal PTA=0.656g) and experimental counterparts are not comparable, and were only marginally considered in this section.

Table 4 Pre-test shake-table loading protocol (PTA = peak table acceleration)

Run #	[-]	0.1	0.2	0.3	1.1	1.2	1.3	2.1	2.2	2.3	3.1	3.2	3.3
PTA	[g]	0.219	0.156	0.156-0.219	0.438	0.313	0.313-0.438	0.656	0.469	0.469-0.656	0.875	0.625	0.625-0.875
Direction	[-]	Y	X	X-Y	Y	X	X-Y	Y	X	X-Y	Y	X	X-Y

The response predicted by the M-DEM before the test resulted in the final damage configuration after run 2.1 depicted in **Figure 8** (d). The damage at this level of shaking, and at other levels which are not shown, indicate that the response was governed by the OOP flexural response of U2 and its interaction with U1 in the Y-direction, as further explained below. Only minor damage (limited also in the test, but underpredicted by the M-DEM) was detected due to the X-shaking.

As in the test, numerical cracks (i.e. shear/tensile joint failures – only cracks wider than 1.5 mm are reported in **Figure 8** (d) and herein chosen as the main indicator for cumulative damage as opposed to that used for the walls of **Figure 7**, difficult to read in this case) revealed the activation of an OOP mechanism in the upper floor of U2, caused by seismic pounding induced by the difference in height with U1. In the first runs (0.1 to 0.3), very minor damage was correctly predicted. Minor to moderate damage characterized the simulated behavior of the second phase (1.1 to 1.3), with IP cracks propagating from the openings of façades 2 and 3 (see **Figure 3**) and at the bottom of the piers of the façade 4 of U2, exhibiting a pronounced OOP rocking response. After run 2.1, the cracks distribution of **Figure 8** (d) appeared, indicating IP damage propagation towards the spandrels of U2 and piers of U1 (which suffered toe-crushing and diagonal shear damage – not observed experimentally), as well as OOP rocking damage of façades 1 and 4 of U2. From 2.2 onward, open cracks continued to widen from previously activated failure mechanisms, leading to extensive damage and near-collapse conditions after run 3.3.

In terms of force-displacement hysteretic response (see **Figure 9** (a)), the M-DEM provided a satisfactory prediction of both peak X and Y-direction base shear, which was slightly overestimated (*rBS*$_X$=1.01, *rBS*$_Y$=1.23). Initial lateral stiffness (calculated at 20% of base shear) was significantly overpredicted (*rK*$_X$=1.59, *rK*$_Y$=1.77), possibly due to the excessive interlocking at corners, which may have increased the coupling among orthogonal walls and thus overestimated the overall box-behavior. As depicted in **Figure** 6(b) indeed, the pre-test model featured complex 3D connections limiting the relative displacement and rotation of orthogonally intersecting walls, providing additional unwanted constraints at corners throughout the walls' heights, as confirmed in the post-test analyses. After run 1.1, lateral stiffness and strength started to decrease significantly leading to more noticeable displacements, albeit underestimating the actual ones as further discussed below, accumulating a residual of about 30 mm in the Y-direction for the roof of U2 (see **Figure 9** (b)). **Figure 9** (c) shows numerical vs experimental comparisons in the form of IDA curves (run 0.1 to 2.1). Interface opening between the units (i.e. the relative displacement among U1 and U2 at the top corners of North and South walls of U1, adjacent to U2) were either underestimated (*x*-direction) or overestimated (*y*-direction up to run 1.3; the final value after run 2.1 underestimates the actual one) by the M-DEM, albeit within reasonable limits before run 1.2 (*rI*$_X$=0.87; ratio among experimental and numerical interface opening along x-direction) and 2.1 (*rI*$_Y$=1.1). Analogous trends were computed for U1 and U2 roof displacements (taken as the average diaphragm value at corners), from which it can be gathered that the M-DEM yielded an underestimate of the response in both the *x*- and y-directions. Further comparisons are available in Tomić et al. (2022).

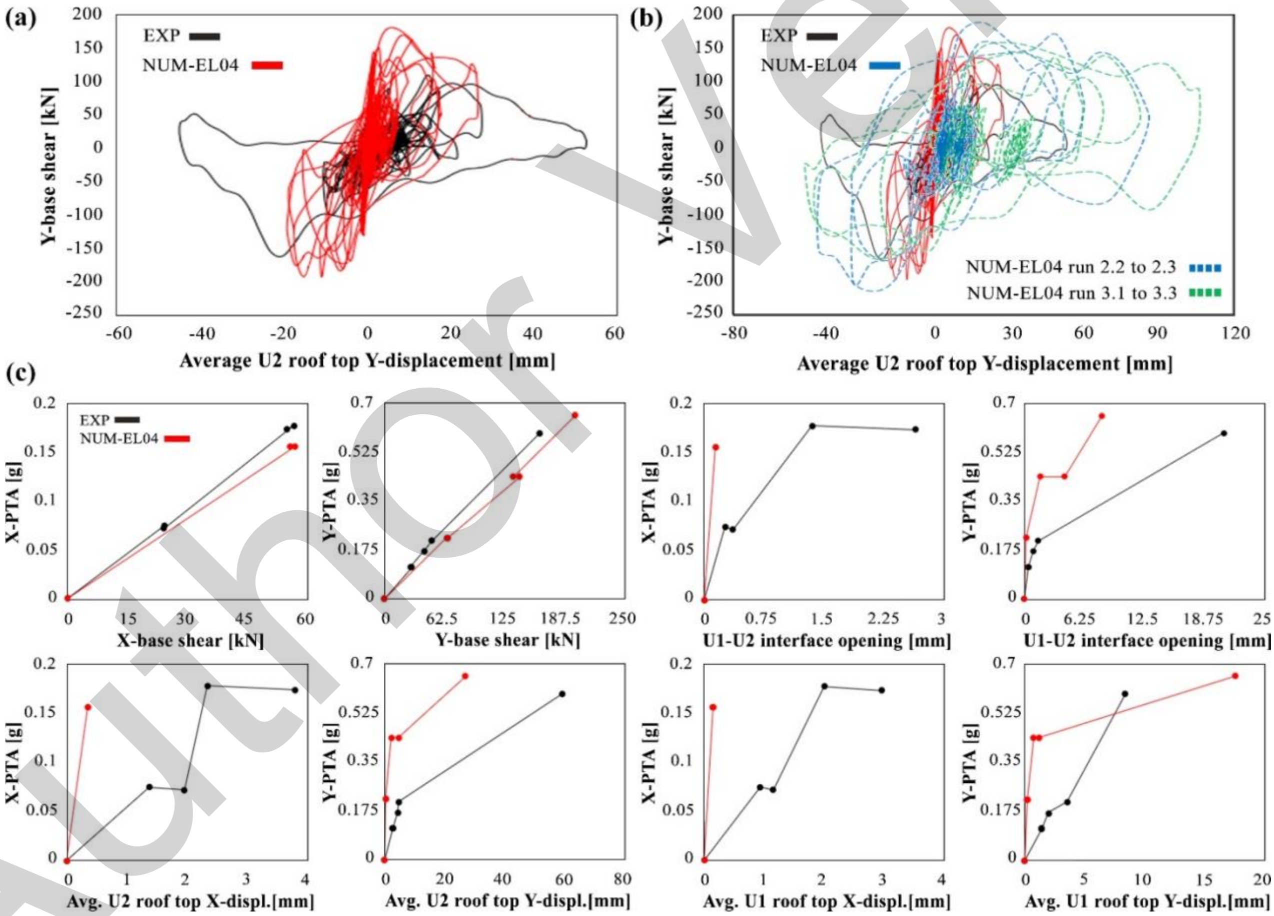

Figure 9 U2 y-direction hysteretic response from (a) run 0.1 to 2.1 and (b) from 2.2 to 3.3, (c) IDA curves

7. POST-TEST IMPROVEMENTS AND RESULTS

Building on the blind prediction M-DEM model and after having analyzed the experimental results and their comparison against the numerical ones, the original modeling strategy was modified to better simulate the experimental behavior. In addition to updating the material properties with post-test data as per **Table 1**, the following tweaks were implemented:

1) As shown in **Figure 4** (c), the placement of irregular stones within walls created voids, typically observed also in the real-world and which can hardly be completely filled with mortar. The irregular shape of stone also meant that contact between units often occurred at discrete points, rather than continuous surfaces. To account for this aspect, which inevitably lowers the overall normal and flexural stiffness of stone masonry members, the normal joint stiffnesses k_n of the zero-thickness interfaces (computed using updated E_m value, see **Table 1**) between FE macro-blocks were decreased by a factor of 10, making them more deformable (considering also that the new E_m is 30% lower than its pre-test counterpart) yet still rigid enough to cause the macro-blocks to be the main source of system deformability. Modifying k_n instead of masonry Young's modulus allowed us to avoid modifying the Feenstra-De Borst crushing model assigned to the FE macro-blocks; the use of an equivalent masonry Young's modulus would have required many cycles of iterative calibration to prevent early crushing failure. Despite the post-test reduction of k_n, the interface springs' shear stiffness k_s was assumed not to vary. Although the rationale of decreasing k_n while keeping k_s constant could be explained by assuming that most of voids and not-properly-filled joints are localized at the vertical interface between stones, further studies on this aspect are certainly needed. This is particularly relevant as it was observed that reducing k_s alongside k_n resulted in spurious IP shear failure modes, especially of U1 walls, not observed experimentally

2) To reduce the lateral stiffness of the model and its box-behavior, corner elements (in blue color in **Figure 10** (a)) replaced the interlocking blocks at the intersection of orthogonal walls. The corner elements are made up of an assembly of rectangular FE solid units, to which the masonry properties are assigned, separated by interface horizontal joints (with the same properties of the M-DEM horizontal spring layers). The layout of the horizontal joints was specified to enable 3D crack propagation around corners, as described in Malomo and DeJong (2021b), where this strategy was recently (after the SERA-AIMS test) validated against a shake-table test on a URM clay brick assembly. The vertical faces of corner elements are connected to M-DEM panels using interface joints with the same properties as the vertical spring layers of the M-DEM (see **Figure 2** (b))

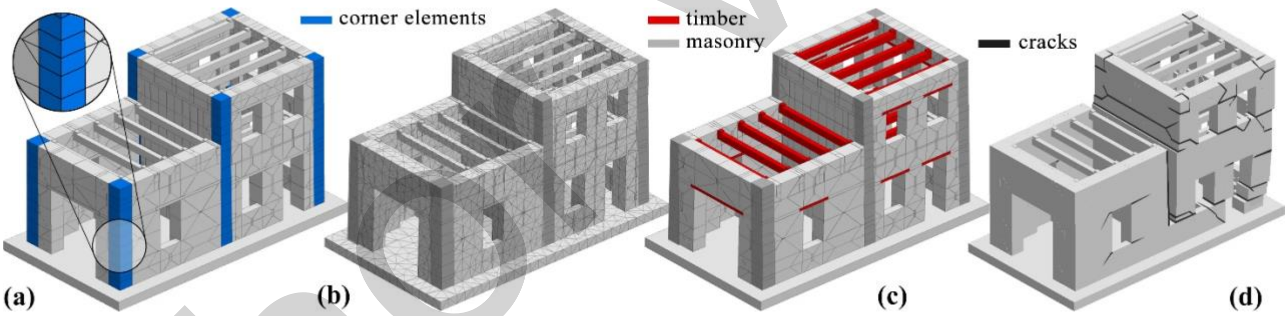

Figure 10 (a) Identification of corner elements, (b) FE mesh, (c) material distribution, (d) predicted damage

3) Mass-proportional damping scheme was maintained in the post-test model, but the fraction of critical damping ζ was reduced from 4% (pre-test) to 3%. This did not impact analysis time, see **Table 3**.

4) The shake-table testing sequence was modified from the pre-test (Table 4) to the actual one. As confirmed by the ratios between nominal and actual PTA values summarized in **Table 5** below, pre-test values were noticeably larger especially in the initial runs. As further discussed below, this may have triggered in the pre-test M-DEM model the activation of inaccurate failure mechanisms at lower displacements (e.g. diagonal failure of the squat piers of U2). As shown in **Table 5** and as for the pre-test model, only unretrofitted runs (0.1 to 2.1) were considered.

Table 5 Post-test shake-table loading protocol and comparison with pre-test one (unretrofitted only)

Run #	[-]	0.1	0.2	0.3	1.1	1.2	1.3	2.1
PTA	[g]	0.113	0.075	0.072-0.114	0.170	0.178	0.174-0.208	0.593
Pre/post PTA ratio	[-]	1.9	2.1	4.3-3.8	2.6	1.8	1.8-1.43	1.1
Direction	[-]	Y	X	X-Y	Y	X	X-Y	Y

During the post-test modeling calibration, the individual effect of the 4 main changes described above was also monitored. The reduction of k_n alone did contribute to achieving the desired U2 rocking-dominated response, while also providing a closer match between numerical and recorded force-displacement hysteretic curves. However, it is only with the simultaneous introduction of corner elements and reduced damping that it was possible to obtain a more reasonable global damage pattern and energy dissipation rates, especially in the last test phases. Applying the latter two tweaks alone did not produce satisfactory results, albeit resulting in conceptually similar yet less noticeable outcomes. Finally, applying the actual testing sequence and shake-table records to the pre-test model, it was observed that the diagonal shear damage of the squat piers of U2 was considerably reduced, making predictions more accurate. This notwithstanding, only the combinations of all the 4 changes above enabled us to achieve the enhanced post-test results discussed in what follows.

As shown in **Figure 10** (d), the results of the post-test simulation exhibit damage that was much more concentrated in U2, as in the actual experiment. The damage propagated as follows. Before run 1.3, U2 suffered only minor damage where an OOP mechanism of façade 4 was activated. Changes in material properties and shaking intensities caused very limited toe-crushing failure in these new analyses. The introduction of corner elements resulted in a better simulation of floor displacements (underestimated in the pre-test simulations) despite lower PTAs, while also limiting the IP damage associated with interlocked corners. This is visible when comparing the force-displacement hysteretic curves displayed in **Figure 11** (a), and even more clear in **Figure 11**(b), where backbone envelope curves are depicted**. Figure 11**(b) shows that the post-test M-DEM model now provides a satisfactory approximation of the overall force-displacement response of U2, with significant improvements with respect to the pre-test simulation. The post-test M-DEM model also better approximates the initial stiffness (rK_X=1.08, rK_Y=1.11), interface opening (rK_X=1.44, rK_Y=1.25) and peak base shear (rBS_X=0.96, rBS_Y=0.98) – see **Figure 11** (c).

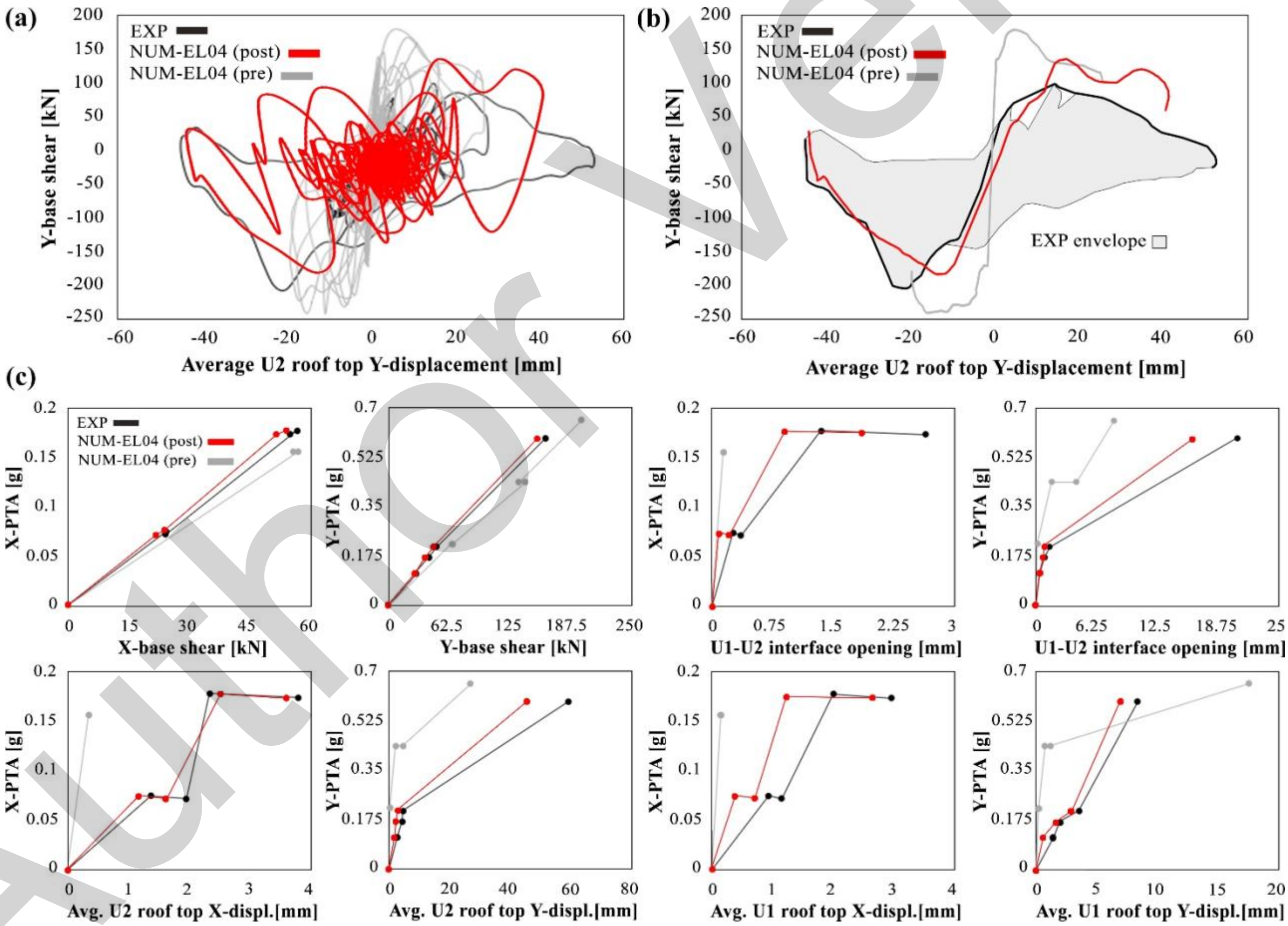

Figure 11 (a) U2 y-dir. hysteretic response (run 0.1 to 2.1), (b) test vs pre/post backbone and (c) IDA curves

8. CONCLUSIONS

Seismic pounding is a complicated phenomenon involving dynamic and impact effects which may cause damage in unreinforced masonry (URM) buildings. Despite recent experimental developments, including the Seismic Testing of Adjacent Interacting Masonry Structures (AIMS) project (sponsored by the Seismology and Earthquake Engineering Research Infrastructure Alliance for Europe, SERA) which is considered in this paper, limited data are available to fully understand the consequences of pounding on the structural safety of non-engineered URM. On the other hand, simulating seismic pounding is challenging using simplified methods originally developed for steel and reinforced concrete systems, which are not readily applicable. As part of the SERA-AIMS blind prediction exercise, this paper describes the development and improvement of the first simplified macro-modeling strategy compatible with the Distinct Element Method, which is naturally suitable to model impacts. Specifically, the work presented in this paper extends the demonstrated capabilities of the Macro-Distinct Element Model (M-DEM) approach, previously used to simulate in-plane (IP) and out-of-plane (OOP) failures of clay and concrete URM, to the modeling of stone masonry and seismic pounding, providing a new analysis solution with acceptable computational cost for both practitioners and researchers.

The pre-test M-DEM model significantly underestimated the floor displacements of the SERA-AIMS specimen, albeit satisfactorily predicting the overall base shear. This is believed to be a direct consequence of the modeling of the connection between orthogonal walls. Relying on interlocking macro-blocks provided too much lateral stiffness, resulting in damage localization (especially in U1) and increased resistance (the pre-test model reached near-collapse conditions only in run 3.3). The dynamic interaction among the units, measured as the relative displacement between them, was also significantly underestimated. The modeling of stone masonry itself also contributed to the underprediction of response obtained by the pre-test M-DEM simulation. Indeed, irregular stone masonry, such as that tested in the SERA-AIMS project, often presents voids and air cavities within the wall thickness, whose reduction effects on normal and flexural stiffness were initially not accounted for numerically. The observation of experimental results and the interpretation of inferred data enabled the following modeling improvements:

- Corner elements were used to replace interlocking corner blocks at orthogonal wall intersections, providing more deformability to the overall system
- Normal stiffnesses of spring layers among FE macro-blocks were decreased to account for imperfect contact conditions due to the heterogeneity of the masonry,
- The fraction of critical damping in the mass-proportional damping scheme used for the analyses was decreased slightly from 4% to 3%

The identification of these key parameters represents key lessons learned, which complement the following primary assumptions made before the test that seemed to have worked well in this modeling exercise:

- A simplified definition of the average slope φ for irregular stone masonry, based on previous experimentally inferred average inclination of cracks in structural URM members, was effective; this aspect deserves to be investigated in more depth for different types of units
- Nonlinear parameters for stone masonry material were effectively selected based on past equivalent test values
- Simplified modeling of timber floors as beam-link assemblies was adequate for IP/OOP loading
- Mass-proportional damping, although not ideal for rocking-governed responses, was found to be the only approach that allowed acceptable computational expense. New research (Vlachakis et al. 2021; Galvez et al. 2022) has recently been published on this topic, which can hopefully contribute to improving this important aspect in future studies.

The post-test implementation of the abovementioned changes, combined with the adoption of updated material properties and loading protocols obtained from actual test data, resulted in a significant improvement of the post-test results in terms of damage distribution and extent, force-displacement hysteretic response, overall deformability, and interface opening. In general, the post-test M-DEM models tended to slightly underestimate experimental outcomes. Future developments include a more thorough investigation of the modeling of the average slope φ when dealing with stone masonry and the influence of different damping schemes, as well as the quantification of the effect of epistemic and material uncertainties on numerical results.

ACKNOWLEDGEMENTS

The authors express their gratitude to all those who practically conducted the test at the National Laboratory for Civil Engineering (LNEC – Lisbon, Portugal), as well as to members of the "Earthquake Engineering and Structural Dynamics" (EESD) research group at EPFL who led the SERA-AIMS project. In particular, the authors would like to thank I. Tomić for his help with the blind prediction and in accessing the test data, where he demonstrated outstanding technical, management and communication skills. Finally, the authors would like to thank three anonymous reviewers, whose insightful comments have contributed to significantly improve the overall quality of this manuscript.

REFERENCES

Abdel Raheem SE, Fooly MYM, Abdel Shafy AGA, et al (2019) Numerical simulation of potential seismic pounding among adjacent buildings in series. Bull Earthq Eng 17:439–471. https://doi.org/10.1007/s10518-018-0455-0

ACI (2019) ACI 318-19. Am Concr Institute, 318-19 Build Code Requir Struct Concr Comment. https://doi.org/10.14359/51716937

Anagnostopoulos SA (1988) Pounding of buildings in series during earthquakes. Earthq Eng Struct Dyn 16:443–456. https://doi.org/10.1002/eqe.4290160311

Antoniou S, Pinho R (2004) SeismoSignal: A computer program for signal processing of strong-motion data

Battaglia L, Ferreira TM, Lourenço PB (2021) Seismic fragility assessment of masonry building aggregates: A case study in the old city Centre of Seixal, Portugal. Earthq Eng Struct Dyn 50:1358–1377. https://doi.org/10.1002/eqe.3405

Bertero V V. (1986) Observations on Structural Pounding. In: The Mexico Earthquakes—1985: Factors Involved and Lessons Learned. pp 264–278

Beyer K (2012) Peak and residual strengths of brick masonry spandrels. Eng Struct 41:533–547. https://doi.org/10.1016/j.engstruct.2012.03.015

Beyer K, Dazio A (2012) Quasi-static cyclic tests on masonry spandrels. Earthq Spectra 28:907–929. https://doi.org/10.1193/1.4000063

Binda L, Fontana A, Mirabella G (1994) Mechanical behavior and stress distribution in multiple-leaf stone walls. In: In Proceedings of the 10th International Brick and Block Masonry Conference. pp 51–59

Çaktı E, Saygılı Ö, Lemos J V., Oliveira CS (2016) Discrete element modeling of a scaled masonry structure and its validation. Eng Struct 126:224–236. https://doi.org/10.1016/j.engstruct.2016.07.044

Calderini C, Cattari S, Lagomarsino S (2010) The use of the diagonal compression test to identify the shear mechanical parameters of masonry. Constr Build Mater 24:677–685. https://doi.org/10.1016/j.conbuildmat.2009.11.001

Chácara C, Cannizzaro F, Pantò B, et al (2018) Assessment of the dynamic response of unreinforced masonry structures using a macroelement modeling approach. Earthq Eng Struct Dyn 47:2426–2446. https://doi.org/10.1002/eqe.3091

Chau KT, Wei XX, Guo X, Shen CY (2003) Experimental and theoretical simulations of seismic poundings between two adjacent structures. Earthq Eng Struct Dyn 32:537–554. https://doi.org/10.1002/eqe.231

Chen SY, Moon FL, Yi T (2008) A macroelement for the nonlinear analysis of in-plane unreinforced masonry piers. Eng Struct 30:2242–2252. https://doi.org/10.1016/j.engstruct.2007.12.001

Cole G, Dhakal R, Carr A, Bull D (2010) Interbuilding pounding damage observed in the 2010 darfield earthquake. Bull New Zeal Soc Earthq Eng 43:382–386. https://doi.org/10.5459/bnzsee.43.4.382-386

Comite Euro-International Du Beton (1990) CEB/FIP Model Code. Des Code. https://doi.org/10.1680/ceb-fipmc1990.35430

Cundall PA (1971) A computer model for simulating progressive large scale movements in blocky rock systems. In: Proc. Symp. Rock Fracture (ISRM), Nancy

Cundall PA (1982) Adaptive density-scaling for time-explicit calculations. In: Numerical Methods in Geomechanics. Edmonton, Canada, pp 23–26

D'Altri AM, Messali F, Rots J, et al (2019) A damaging block-based model for the analysis of the cyclic behaviour of full-scale masonry structures. Eng Fract Mech 209:423–448. https://doi.org/10.1016/j.engfracmech.2018.11.046

D'Altri AM, Sarhosis V, Milani G, et al (2020) Modeling Strategies for the Computational Analysis of Unreinforced Masonry Structures: Review and Classification. Arch Comput Methods Eng 27:1153–1185. https://doi.org/10.1007/s11831-019-09351-x

Davis RO (1992) Pounding of buildings modelled by an impact oscillator. Earthq Eng Struct Dyn 21:253–274. https://doi.org/10.1002/eqe.4290210305

Degli Abbati S, D'Altri AM, Ottonelli D, et al (2019) Seismic assessment of interacting structural units in complex historic masonry constructions by nonlinear static analyses. Comput Struct 213:51–71. https://doi.org/10.1016/j.compstruc.2018.12.001

DeJong MJ (2009) Seismic Assessment Strategies for Masonry Structures. PhD Thesis, Massachusetts Inst

Technol United States

Elmenshawi A, Shrive N (2015) Assessment of multi-wythe stone masonry subjected to seismic hazards. J Earthq Eng 19:85–106. https://doi.org/10.1080/13632469.2014.940631

Elmenshawi A, Sorour M, Mufti A, et al (2010) Damping mechanisms and damping ratios in vibrating unreinforced stone masonry. Eng Struct 32:3269–3278. https://doi.org/10.1016/j.engstruct.2010.06.016

Elwardany H, Seleemah A, Jankowski R (2017) Seismic pounding behavior of multi-story buildings in series considering the effect of infill panels. Eng Struct 144:139–150. https://doi.org/10.1016/j.engstruct.2017.01.078

Erdogan YS, Kocatürk T, Demir C (2019) Investigation of the Seismic Behavior of a Historical Masonry Minaret Considering the Interaction with Surrounding Structures. J Earthq Eng 23:112–140. https://doi.org/10.1080/13632469.2017.1309725

Eurocode CEN (2005) 6: Design of masonry structures, Part 1--1: General rules for reinforced and unreinforced masonry structures. Eur Comm Stand Belgium

Favvata MJ, Naoum MC, Karayannis CG (2013) Earthquake induced interaction between RC frame and steel frame structures. WIT Trans Built Environ 134:839–851. https://doi.org/10.2495/SAFE130741

Feenstra PH, De Borst R (1996) A composite plasticity model for concrete. Int J Solids Struct 33:707–730. https://doi.org/10.1016/0020-7683(95)00060-N

Filiatrault A, Wagner P, Cherry S (1996) An experimental study on the seismic pounding of buildings. In: Eleventh World Conference on Earthquake Engineering

Formisano A, Massimilla A (2018) A Novel Procedure for Simplified Nonlinear Numerical Modeling of Structural Units in Masonry Aggregates. Int J Archit Herit 12:1162–1170. https://doi.org/10.1080/15583058.2018.1503365

Galvez F, Sorrentino L, Dizhur D, Ingham JM (2022) Damping considerations for rocking block dynamics using the discrete element method. Earthq Eng Struct Dyn 51:935–957. https://doi.org/10.1002/eqe.3598

Gattesco N, Macorini L (2014) In-plane stiffening techniques with nail plates or CFRP strips for timber floors in historical masonry buildings. Constr Build Mater 58:64–76. https://doi.org/10.1016/j.conbuildmat.2014.02.010

Ghandil M, Aldaikh H (2017) Damage-based seismic planar pounding analysis of adjacent symmetric buildings considering inelastic structure–soil–structure interaction. Earthq Eng Struct Dyn 46:1141–1159. https://doi.org/10.1002/eqe.2848

Griffith MC, Vaculik J, Lam NTK, et al (2007) Cyclic testing of unreinforced masonry walls in two-way bending. Earthq Eng Struct Dyn 36:801–821. https://doi.org/10.1002/eqe.654

Grillanda N, Valente M, Milani G, et al (2020) Advanced numerical strategies for seismic assessment of historical masonry aggregates. Eng Struct 212:110441. https://doi.org/10.1016/j.engstruct.2020.110441

Guerrini G, Senaldi I, Graziotti F, et al (2019) Shake-Table Test of a Strengthened Stone Masonry Building Aggregate with Flexible Diaphragms. Int J Archit Herit 13:1078–1097. https://doi.org/10.1080/15583058.2019.1635661

Hao H (2015) Analysis of seismic pounding between adjacent buildings. Aust J Struct Eng 16:208–225. https://doi.org/10.1080/13287982.2015.1092684

Hosseini SH, Naderpour H, Vahdani R, Jankowski R (2022) Evaluation of pounding effects between reinforced concrete frames subjected to far-field earthquakes in terms of damage index. Bull Earthq Eng 20:1219–1245. https://doi.org/10.1007/S10518-021-01259-X/FIGURES/26

Itasca Consulting Group Inc. (2013) 3DEC. Three Dimensional Distinct Element Code

Jankowski R (2010) Experimental study on earthquake-induced pounding between structural elements made of different building materials. Earthq Eng Struct Dyn 39:343–354. https://doi.org/10.1002/eqe.941

Karbassi A, Nollet M-J (2013) Performance-based seismic vulnerability evaluation of masonry buildings using applied element method in a nonlinear dynamic-based analytical procedure. Earthq Spectra 29:399–426

Kasai K, Maison BF (1997) Building pounding damage during the 1989 Loma Prieta earthquake. Eng Struct 19:195–207. https://doi.org/10.1016/S0141-0296(96)00082-X

Khatiwada S, Chouw N, Butterworth JW (2013) Evaluation of numerical pounding models with experimental validation. Bull New Zeal Soc Earthq Eng 46:117–130. https://doi.org/10.5459/bnzsee.46.3.117-130

Kim J, Lorenzoni F, Salvalaggio M, Valluzzi MR (2021) Seismic vulnerability assessment of free-standing massive masonry columns by the 3D Discrete Element Method. Eng Struct 246:113004.

https://doi.org/10.1016/j.engstruct.2021.113004
Lemos J V., Campos Costa A (2017a) Simulation of Shake Table Tests on Out-of-Plane Masonry Buildings. Part (V): Discrete Element Approach. Int J Archit Herit 11:117–124. https://doi.org/10.1080/15583058.2016.1237587
Lemos J V., Campos Costa A (2017b) Simulation of Shake Table Tests on Out-of-Plane Masonry Buildings.
Lourenço PB, Pereira JM (2018) Seismic retrofitting project : recommendations for advanced modeling of historic earthen sites. Getty Res Inst 1–78
Luzi L, Lanzano G, Felicetta C, et al (2020) Engineering Strong Motion Database (ESM) (Version 2.0). Ist Naz di Geofis e Vulcanol 10:
Magenes G, Calvi GM (1997) In-plane seismic response of brick masonry walls. Earthq Eng Struct Dyn 26:1091–1112. https://doi.org/10.1002/(SICI)1096-9845(199711)26:11<1091::AID-EQE693>3.0.CO;2-6
Malomo D, DeJong MJ (2021a) A Macro-Distinct Element Model (M-DEM) for out-of-plane analysis of unreinforced masonry structures. Eng Struct 244:. https://doi.org/10.1016/j.engstruct.2021.112754
Malomo D, DeJong MJ (2021b) A Macro-Distinct Element Model (M-DEM) for simulating in-plane/out-of-plane interaction and combined failure mechanisms of unreinforced masonry structures. Earthq Eng Struct Dyn. https://doi.org/10.1002/eqe.3591
Malomo D, DeJong MJ (2021c) A Macro-Distinct Element Model (M-DEM) for simulating the in-plane cyclic behavior of URM structures. Eng Struct 227:111428. https://doi.org/10.1016/j.engstruct.2020.111428
Malomo D, DeJong MJ, Penna A (2019a) Influence of Bond Pattern on the in-plane Behavior of URM Piers. Int J Archit Herit. https://doi.org/10.1080/15583058.2019.1702738
Malomo D, DeJong MJ, Penna A (2019b) Distinct element modelling of the in-plane cyclic response of URM walls subjected to shear-compression. Earthq Eng Struct Dyn 48:1322–1344. https://doi.org/10.1002/eqe.3178
Malomo D, Mehrotra A, DeJong MJ (2021) Distinct element modeling of the dynamic response of a rocking podium tested on a shake table. Earthq Eng Struct Dyn 50:1469–1475. https://doi.org/10.1002/eqe.3404
Malomo D, Pinho R, Penna A (2020a) Simulating the shake table response of unreinforced masonry cavity wall structures tested to collapse or near-collapse conditions. Earthq Spectra 36:554–578. https://doi.org/10.1177/8755293019891715
Malomo D, Pinho R, Penna A (2020b) Applied Element Modelling of the Dynamic Response of a Full-Scale Clay Brick Masonry Building Specimen with Flexible Diaphragms. Int J Archit Herit 14:1484–1501. https://doi.org/10.1080/15583058.2019.1616004
Maniatakis CA, Spyrakos CC, Kiriakopoulos PD, Tsellos KP (2018) Seismic response of a historic church considering pounding phenomena. Bull Earthq Eng 16:2913–2941. https://doi.org/10.1007/s10518-017-0293-5
Miari M, Choong KK, Jankowski R (2021) Seismic Pounding Between Bridge Segments: A State-of-the-Art Review. Arch Comput Methods Eng 28:495–504. https://doi.org/10.1007/s11831-019-09389-x
Milosevic J, Gago AS, Lopes M, Bento R (2013) Experimental assessment of shear strength parameters on rubble stone masonry specimens. Constr Build Mater 47:1372–1380. https://doi.org/10.1016/j.conbuildmat.2013.06.036
NTC (2018) Decreto Ministeriale 17/1/2018: Norme Tecniche per le Costruzioni. Minist Infrastructures Transp Gazz Uff n42 20/2/2008 [in Ital
Pelà L, Aprile A, Benedetti A (2009) Seismic assessment of masonry arch bridges. Eng Struct 31:1777–1788
Penna A, Lagomarsino S, Galasco A (2014) A nonlinear macroelement model for the seismic analysis of masonry buildings. Earthq Eng Struct Dyn 43:159–179
Penna A, Senaldi IE, Galasco A, Magenes G (2016) Numerical Simulation of Shaking Table Tests on Full-Scale Stone Masonry Buildings. Int J Archit Herit 10:146–163. https://doi.org/10.1080/15583058.2015.1113338
Penner O, Elwood KJ (2016) Out-of-plane dynamic stability of unreinforced masonry walls in one-way bending: Shake table testing. Earthq Spectra 32:1675–1697. https://doi.org/10.1193/011415EQS009M
Pujades LG, Barbat AH, González-Drigo R, et al (2012) Seismic performance of a block of buildings representative of the typical construction in the Eixample district in Barcelona (Spain). Bull Earthq Eng 10:331–349. https://doi.org/10.1007/s10518-010-9207-5
Pulatsu B, Bretas EM, Lourenço PB (2016) Discrete element modeling of masonry structures: Validation and application. Earthq Struct 11:563–582. https://doi.org/10.12989/eas.2016.11.4.563

Pulatsu B, Erdogmus E, Lourenço PB, et al (2020) Discontinuum analysis of the fracture mechanism in masonry prisms and wallettes via discrete element method. Meccanica 55:505–523. https://doi.org/10.1007/s11012-020-01133-1

Pulatsu B, Erdogmus E, Lourenço PB, Quey R (2019) Simulation of uniaxial tensile behavior of quasi-brittle materials using softening contact models in DEM. Int J Fract 217:105–125. https://doi.org/10.1007/s10704-019-00373-x

SA (2007) AS 1170.4-2007. Stand Aust Struct Des actions, Part 4 Earthq actions Aust

Senaldi I, Guerrini G, Scherini S, et al (2018) Natural stone masonry characterization for the shaking-table test of a scaled building specimen. In: Proceedings of the 10th International Masonry Conference. pp 1530–1545

Senaldi I, Magenes G, Penna A (2010) Numerical investigations on the seismic response of masonry building aggregates. Adv Mater Res 133–134:715–720. https://doi.org/10.4028/www.scientific.net/AMR.133-134.715

Sferrazza Papa G, Tateo V, Parisi MA, Casolo S (2021) Seismic response of a masonry church in Central Italy: the role of interventions on the roof. Bull Earthq Eng 19:1151–1179. https://doi.org/10.1007/s10518-020-00995-w

Sha B, Tao T, Asce AM, et al (2020) Pounding Analysis of Isolated Girder Bridge under Nonpulse and Pulse-Like Earthquakes. J Perform Constr Facil 34:04020062. https://doi.org/10.1061/(ASCE)CF.1943-5509.0001468

So E, Spence R (2013) Estimating shaking-induced casualties and building damage for global earthquake events: A proposed modelling approach. Bull Earthq Eng 11:347–363. https://doi.org/10.1007/s10518-012-9373-8

Sołtysik B, Falborski T, Jankowski R (2017) Preventing of earthquake-induced pounding between steel structures by using polymer elements – experimental study. Procedia Eng 199:278–283. https://doi.org/10.1016/J.PROENG.2017.09.029

Sołtysik B, Jankowski R (2016) Earthquake-induced pounding between asymmetric steel buildings. Geotech Geol Earthq Eng 40:255–261. https://doi.org/10.1007/978-3-319-14246-3_23

Tomić I, Penna A, DeJong M, et al (2021) Seismic testing of adjacent interacting masonry structures. 12th Int. Conf. Struct. Anal. Hist. Constr.

Tomić I, Penna A, DeJong MJ, et al (2022) Shake-table testing of a half-scale stone masonry building aggregate. Bull Earthq Eng - under review

Van der Pluijm R (1993) Shear behaviour of bed joints. In: Proceedings of the 6th North American Masonry Conference. Philadelphia, USA

Van Der Pluijm R (1997) Non-linear behaviour of masonry under tension. Heron 42:25–48

Vanin F, Penna A, Beyer K (2020a) Equivalent-Frame Modeling of Two Shaking Table Tests of Masonry Buildings Accounting for Their Out-Of-Plane Response. Front Built Environ 6:42. https://doi.org/10.3389/fbuil.2020.00042

Vanin F, Penna A, Beyer K (2020b) A three-dimensional macroelement for modelling the in-plane and out-of-plane response of masonry walls. Earthq Eng Struct Dyn 49:1365–1387. https://doi.org/10.1002/eqe.3277

Vasconcelos G, Lourenço PB (2009) In-Plane Experimental Behavior of Stone Masonry Walls under Cyclic Loading. J Struct Eng 135:1269–1277. https://doi.org/10.1061/(asce)st.1943-541x.0000053

Vlachakis G, Giouvanidis AI, Mehrotra A, Lourenço PB (2021) Numerical Block-Based Simulation of Rocking Structures Using a Novel Universal Viscous Damping Model. J Eng Mech 147:04021089. https://doi.org/10.1061/(asce)em.1943-7889.0001985

Won JH, Mha HS, Kim SH (2015) Effects of the earthquake-induced pounding upon pier motions in the multi-span simply supported steel girder bridge. Eng Struct 93:1–12. https://doi.org/10.1016/j.engstruct.2015.03.010

Zhang S, Hofmann M, Beyer K (2018) A 2D typology generator for historical masonry elements. Constr Build Mater 184:440–453. https://doi.org/10.1016/j.conbuildmat.2018.06.085

STATEMENTS & DECLARATIONS

Funding

The authors declare that no funds, grants, or other support were received during the preparation of this manuscript.

Competing Interests

The authors have no relevant financial or non-financial interests to disclose.

Author Contributions

All authors contributed to the study conception and design. Material preparation, data collection and analysis were performed by Daniele Malomo. The first draft of the manuscript was written by Daniele Malomo and Matthew J. DeJong commented on previous versions of the manuscript. All authors read and approved the final manuscript.

Data Availability

The datasets presented in this study are available from the corresponding author on reasonable request.